THE ASTROPHYSICAL JOURNAL, 531:312–320, 2000 March 1

GAS-PHASE ELECTRONIC SPECTRA OF CARBON-CHAIN RADICALS COMPARED WITH DIFFUSE INTERSTELLAR BAND OBSERVATIONS

T. MOTYLEWSKI, H. LINNARTZ, O. VAIZERT, AND J. P. MAIER[1]
Institute for Physical Chemistry, Klingelbergstrasse 80, CH-4056 Basel, Switzerland; motyl@stan.chemie.unibas.ch, Henricus.Linnartz@unibas.ch, olga@stan.chemie.unibas.ch, Maier@ubaclu.unibas.ch

G. A. GALAZUTDINOV AND F. A. MUSAEV
Special Astrophysical Observatory, Nizhnij Arkhyz 357147, Russia; gala@sao.ru, faig@sao.ru

J. KREŁOWSKI
Center for Astronomy, Nicholas Copernicus University, Gagarina 11, Pl-87-100 Toruń, Poland; jacek@astri.uni.torun.pl

G. A. H. WALKER[2]
Physics and Astronomy Department, University of British Columbia, Vancouver, B.C. Canada V6T 1Z4; walker@astro.ubc.ca

AND

D. A. BOHLENDER[2]
Herzberg Institute of Astrophysics, Dominion Astrophysical Observatory, 5071 West Saanich Road, Victoria, B.C. Canada V8X 4M6; David.Bohlender@hia.nrc.ca

Received 1999 August 31; accepted 1999 October 14

ABSTRACT

This paper compares laboratory gas-phase spectra of neutral and cationic linear carbon-chain radicals with astronomical diffuse interstellar band (DIB) spectra. The origin bands of the strong electronic transitions of the studied species, $C_{2n}H$ ($n = 3$–6), $HC_{2n}H^+$ ($n = 2$–4), $NC_{2n-2}N^+$ ($n = 3$, 4), do not coincide with detectable DIBs, except for $HC_{2n-1}N^+$ ($n = 3$), which possibly matches a weak feature. It is concluded that the column densities of these species through the observed diffuse clouds are below 2×10^{12} cm^{-2}. The profile change and the shift of the maxima of the absorption bands with temperature are illustrated. The relation to radio-astronomical detection of carbon chains in diffuse media is also discussed.

Subject headings: ISM: lines and bands — ISM: molecules

1. INTRODUCTION

Diffuse interstellar bands (DIBs) were discovered nearly 80 years ago at Lick Observatory, when Heger (1922) reported two "stationary" absorption features near 5780 and 5797 Å in several spectroscopic binaries. The interstellar nature of strong DIBs was established by Merrill (1934, 1936), Beals & Blanchet (1937), York (1971), and Herbig (1975). Since then, more than 200 DIBs have been reported, and as the sensitivity of optical techniques improves, their number continues to grow (Krełowski, Sneden, & Hiltgen 1995).

Various forms of matter have been proposed as possible carriers, from dust grains (Merrill et al. 1937) to both simple and rather complicated gas-phase molecules (Tielens & Snow 1995). The latter range from molecular hydrogen (Sorokin et al. 1998) to polycyclic hydrocarbons and their cations (Leger et al. 1987 and references therein; Crawford, Tielens, & Allamandola 1985) and fullerenes (Kroto & Jura 1992). It is now commonly believed that most DIBs originate from carbon-bearing molecules.

The hypothesis that linear carbon molecules, C_n, may be potential DIB carriers was formulated by Douglas (1977). The detection by radio astronomy of numerous linear carbon chains in dark clouds (McCarthy et al. 1997) has strengthened the belief that electronic transitions of such species may be involved in DIB absorptions. The first experimental signs came from absorption measurements of the electronic transitions of mass-selected carbon chains in the neon matrix (Fulara et al. 1993). The best indication is the recent laboratory observation of the electronic $^2\Pi_u \leftarrow X^2\Pi_g$ spectrum of C_7^- in the gas phase by Tulej et al. (1998). The origin band and the prominent vibronic bands show matches with tabulated DIBs, within a ± 2 Å limit. A more detailed comparison with new astronomical data is the subject of two articles (Galazutdinov, Krełowski, & Musaev 1999a and McCall, York, & Oka 1999). Guided by the identification of the transitions of a variety of carbon chains in neon matrices (Maier 1998), the gas-phase spectra have recently been measured for several neutral (Linnartz, Motylewski, & Maier 1998), negatively charged (Zhao et al. 1996; Ohara, Shiromaru, & Achiba 1997; Tulej et al. 1998), and positively charged (Sinclair et al. 1999b) carbon-chain radicals.

Rotational resolution routinely achieved in the laboratory is not likely in the astronomical spectra because of Doppler broadening, but the rotational profile should be preserved. Data acquired by Kerr et al. (1998) with resolving power $R = 600{,}000$ on λ5797 DIBs resemble the rotational contour of an unresolved P, Q, and R-branch. It is expected that these interstellar features should be free of Doppler splitting, since only nearby, bright stars are used. These are most likely obscured by just one cloud, which is proved by the narrow width of interstellar atomic lines (Na I, K I), which in the best case is 0.05 Å. The surveys of DIB profiles between 5600 and 7000 Å by Krełowski & Schmidt (1997) and Galazutdinov et al. (1999b) with $R = 60{,}000$ and 45,000, respectively, demonstrate that in most DIBs some substructure can be seen. This suggests that gas-phase molecules are very likely involved.

[1] Author to whom correspondence should be addressed.

[2] Visiting Astronomer, Canada-France-Hawaii Telescope, operated by the National Research Council of Canada, the Centre National de la Recherche Scientifique of France, and the University of Hawaii.

TABLE 1

BASIC STELLAR DATA

HD/BD Number	Spectral Type	V	$B-V$	$E(B-V)$	$v \sin i$	Observatory
2905	B1 Iae	4.16	+0.14	0.33	62	CFHT
23180	B1 III	3.82	+0.06	0.32	85	SAO/TE
24398	B1 Ib	2.85	+0.12	0.31	59	CFHT
24912	O7e	4.04	+0.01	0.30	216	CFHT
25638	B0 III	6.99	+0.42	0.72	258	TE
167971	O8/O9	7.5	+0.77	1.05	...	TE
168607	O+	8.29	+1.60	1.88	...	SAO/TE
183143	B7 Ia	6.84	+1.27	1.28	60	TE
186745	B8 Ia	7.0	+0.93	1.00	...	TE
190603	B1.5 Iae	5.62	+0.56	0.73	32	SAO/TE
195592	O9.5 Ia	7.08	+0.87	1.11	...	SAO
198478	B3 Iae	4.84	+0.41	0.54	35	CFHT
207198	O9 IIe	5.95	+0.31	0.54	76	SAO/TE
210839	O6 Iab	5.06	+0.23	0.52	285	SAO/TE/CFHT
BD +40°4220	O7e	9.10	+1.67	1.96	...	TE

This paper presents a comparison of recently obtained gas-phase spectra of electronic transitions of linear carbon-chain radicals by cavity-ring-down spectroscopy to new echelle spectra of reddened stars. We discuss the points that must be kept in mind in comparing the laboratory and astronomical spectra, in particular the temperature dependence of the band profiles. The necessity of searching for the DIB features in the directions of several reddened stars is also illustrated. The upper limits for the column density of the studied carbon chains are estimated from the two sets of data.

2. LABORATORY GAS-PHASE SPECTRA

The origin band of the $^2\Pi \leftarrow X^2\Pi$ electronic transition for the carbon-chain radicals studied here is observed in the 5000–8000 Å range using cavity-ring-down laser absorption spectroscopy. The emission spectra of the cationic species have been observed before, but at lower resolution (Maier 1982 and references therein). In the current experiment, the molecules are produced in a pulsed (30 Hz) supersonic plasma generated by discharge in 0.2%–0.5% HCCH and/or NCCN in He mixtures (backing pressure of 10 bar) in the throat of a 30 mm long and 100–300 μm wide slit jet (Motylewski & Linnartz 1999). Rotational temperatures of 10–30 K are obtained. Tunable light (0.15 or 0.035 cm^{-1} bandwidth) from an excimer pumped-dye laser is focused into a high-Q optical cavity a few millimeters below the slit. Light escaping from the cavity is detected by a photomultiplier, and the exponential decay is monitored by an oscilloscope. Several ring-down events are averaged at each wavelength before the digitized data are downloaded to a workstation. Typical ring-down times of 30–50 μs are

TABLE 2

LABORATORY AND ASTRONOMICAL DATA OF CARBON-CHAIN RADICALS WITH INFERRED UPPER LIMITS OF THE COLUMN DENSITY, N_{max}, IN DIFFUSE CLOUDS TOWARD SELECTED STARS

	LABORATORY				ASTRONOMICAL			
CHAIN	λ_{air} (Å)	Reference	f_{0-0}[a]	FWHM (Å)	Star	rms	$W_{\lambda,max}$	N_{max} (10^{12} cm^{-2})
C_6H	5265.756 (3)[b]	1	0.06	1.0	HD 190603	0.0043	0.021	1.43
					HD 207198	0.0032	0.016	1.09
C_8H	6258.66 (8)[c]	2	0.08	1.7	HD 210839	0.0017	0.014	0.50
					HD 207198	0.0037	0.031	1.12
$C_{10}H$	7140.9 (5)[c]	2	0.10	4.0	HD 207198	0.0036	0.072	1.59
					HD 210839	0.0044	0.088	1.95
$C_{12}H$	7904.5 (3)[c]	3	0.12	2.8	HD 210839	0.0066	0.092	1.39
					HD 207198	0.0076	0.106	1.60
HC_4H^+	5068.650 (3)[b]	3, 4	0.04	2.0	HD 207198	0.0046	0.046	5.06
HC_6H^+	6002.138 (3)[b]	3, 5	0.06	1.2	HD 210839	0.0015	0.009	0.47
HC_8H^+	7067.82 (2)[b]	3, 4	0.08	1.9	HD 207198	0.0036	0.034	0.96
					BD +40°4220	0.0058	0.055	1.55
NC_4N^+	5957.738 (3)[b]	3, 6	0.06	1.4	HD 210839	0.005[d]	0.007[d]	0.37
NC_6N^+	6557.52 (3)[b]	3	0.08	1.2	Obscured by Hα line			
HC_5N^+	5819.27 (2)[b]	3, 6	0.06	1.6	HD 207198		0.011[e]	0.61

[a] The f_{0-0} values are scaled using the experimentally determined value of HC_4H^+ (see text).
[b] Band origin.
[c] Band maximum.
[d] Minimum detectable absorption estimated visually.
[e] W_λ for observed λ5819 DIB.

REFERENCES—(1) Linnartz et al. (1998); (2) Linnartz et al. (1999); (3) this work; (4) Allan et al. (1976); (5) Sinclair et al. (1999b); (6) Sinclair et al. (1999a).

equivalent to an effective absorption path length through the supersonic expansion of about 1 km. The averaged ring-down time as a function of the laser frequency yields the spectral information. The spectra are calibrated via I_2 or He I, Ar I, or Ne I absorption lines that are recorded simultaneously. Except for the C_8H, $C_{10}H$, and $C_{12}H$ species, rotational structure is resolved in all spectra. However, this is evident in only some of the figures, where the wavelength scale is not too coarse.

All open-shell species studied contain an even number of C + N atoms. The spin-orbit coupling yields two substates, $^2\Pi_{3/2}$ and $^2\Pi_{1/2}$, with the $\Omega = 3/2$ component at lower energy; i.e., the spin-orbit coupling constant A is negative. Typical A values are ~ -30 cm^{-1}. At a diffuse cloud temperature of about 30 K, the population is mostly in the vibrationless level of the $^2\Pi_{3/2}$ ground state ($\sim$80%). Thus, only the astrophysically relevant $^2\Pi_{3/2} \leftarrow X^2\Pi_{3/2}$ transition is considered here.

3. ASTRONOMICAL DATA

Most of the astronomical spectra were acquired with a new coudé echelle spectrometer (Musaev et al. 1999) fed by the 2 m telescope of the Terskol Observatory (TE), on the top of peak Terskol in the northern Caucasus. The spectrometer, working with a Wright Instruments CCD 1242 × 1152 matrix (pixel size 22.5 μm × 22.5 μm) camera, covers in a single exposure the range 3500–10100 Å, with $R = 45{,}000$. Additional data have been obtained with a similar spectrometer (Musaev 1993, 1996) attached to the 1 m telescope of the Russian Special Astrophysical Observatory (SAO), and with the Gecko coudé échellette spectrograph on the Canada-France-Hawaii Telescope (CFHT).

The TE and SAO echelle spectra were reduced using the DECH code (Galazutdinov 1992), which allows flat-field division, bias/background subtraction, one-dimensional spectrum extraction from two-dimensional images, correction for diffuse light, spectrum addition, and excision of cosmic-ray features. Furthermore, it allows the location of a fiducial continuum and measurements of the line equivalent widths, line positions, and shifts. The covered spectral range contains strong and well-identified Ca II, Ca I, Na I, and K I atomic interstellar lines, which leads to precise and on-line determination of the radial velocities of the intervening interstellar clouds.

The Gecko spectrograph was fed by the red coudé mirror train and objective triplet, and the red-optimized Richardson image slicer, collimator, and camera mirrors, with the thinned, backside-illuminated Loral 5 CCD with 15 μm^2 pixels. The Th/Ar comparison arc spectra taken before and after each spectrograph wavelength reconfiguration had typical FWHM of 2.9 pixels, which corresponds to resolutions of $R = 83{,}000$ at 6000 Å.

Table 1 characterizes the sample of target stars, i.e., HD or BD numbers, spectral types, luminosity classes, magnitudes, color indices or excesses, and rotational velocities. It indicates which of the three spectrometers was used. The targets are of different spectral types to facilitate the distinc-

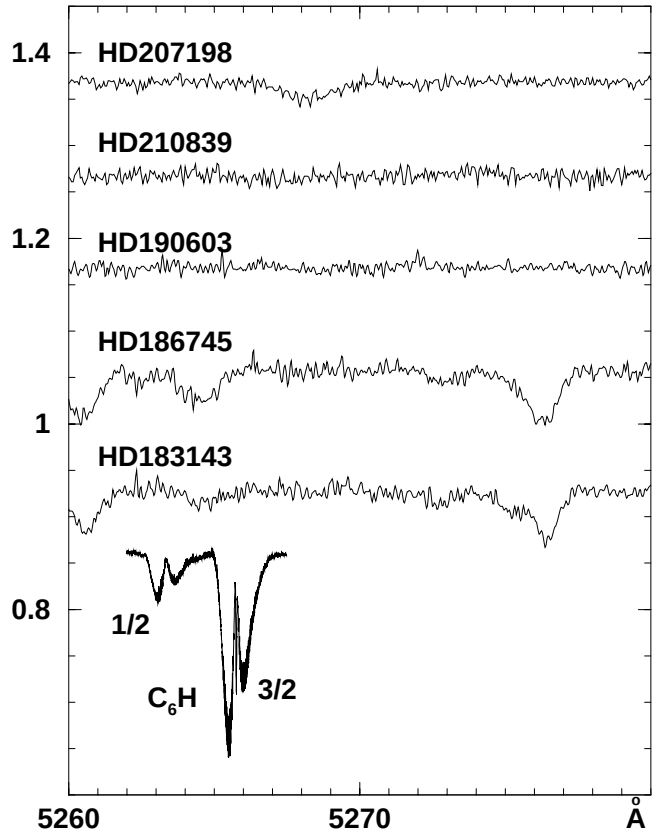

FIG. 1.—Origin band of the $^2\Pi \leftarrow X^2\Pi$ electronic transition of C_6H in the gas phase (*bottom*) compared to astronomical spectra measured toward five different stars. The absorption features observed in the latter are stellar lines.

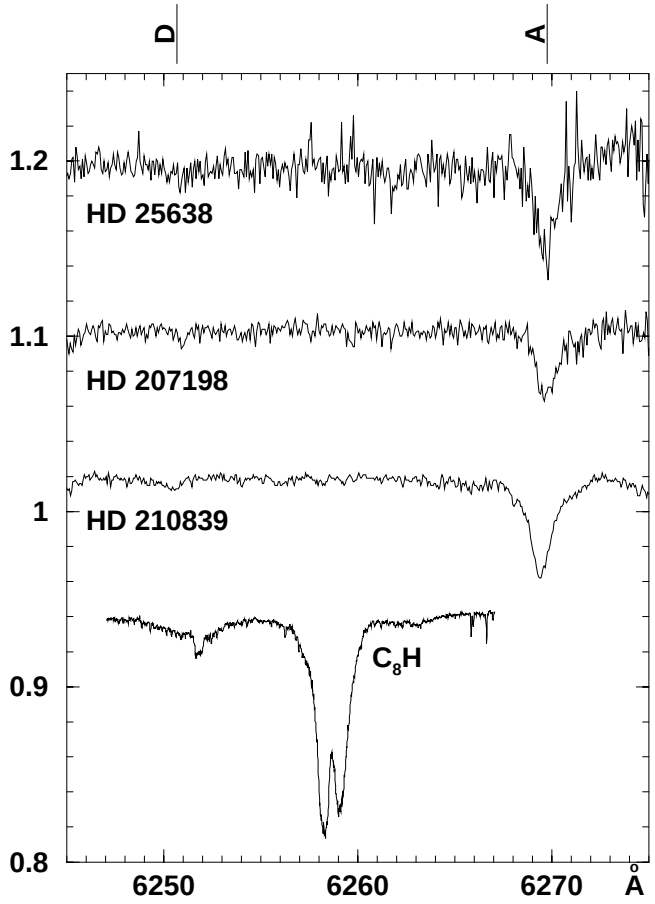

FIG. 2.—Origin band of the $^2\Pi \leftarrow X^2\Pi$ electronic transition of C_8H in the gas phase (*bottom*) compared to astronomical spectra measured toward three different stars.

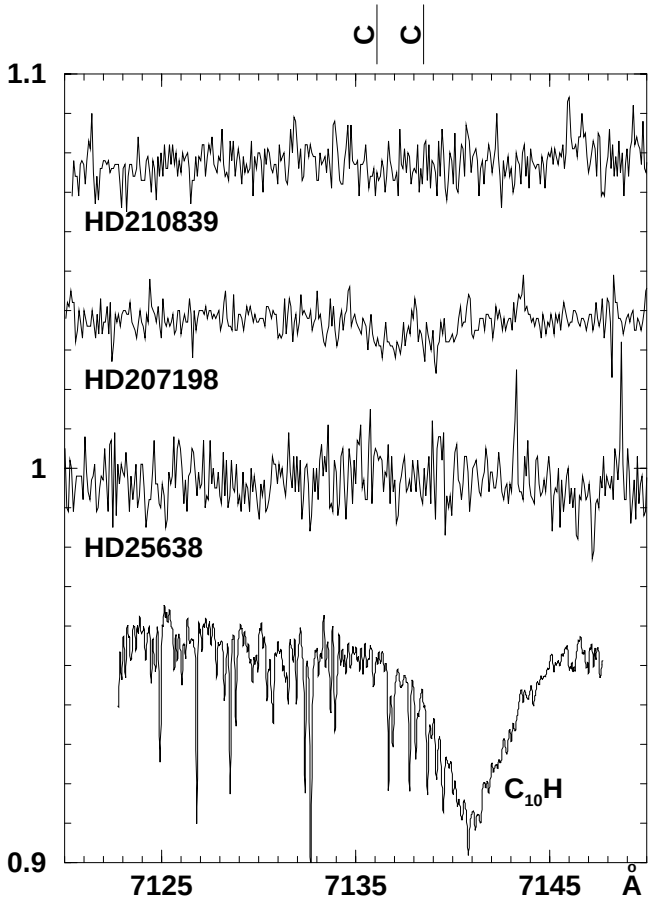

FIG. 3.—Origin band of the $^2\Pi \leftarrow X^2\Pi$ electronic transition of $C_{10}H$ in the gas phase (*bottom*) compared to astronomical spectra measured toward three different stars.

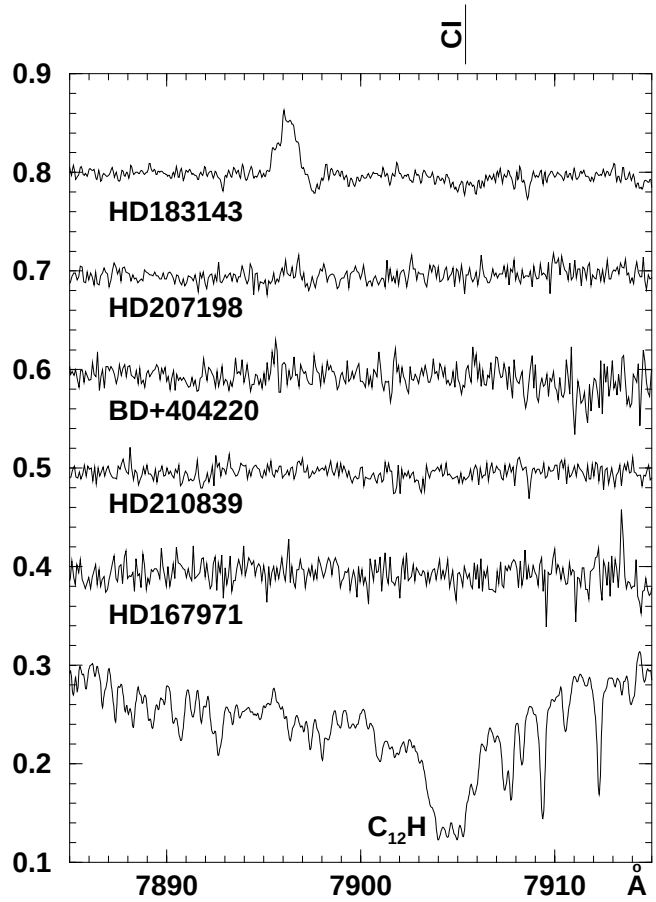

FIG. 4.—Origin band of the $^2\Pi \leftarrow X^2\Pi$ electronic transition of $C_{12}H$ in the gas phase (*bottom*) compared to astronomical spectra measured toward five different stars.

tion between interstellar features and possible stellar lines. The sample was intentionally limited to a set of moderately and heavily reddened stars, some of which (HD 23180, HD 207198, and HD 210839) are known as sources of exceptionally strong DIBs. The CFHT data concern only moderately reddened stars, likely to be observed through single clouds, because the observations were focused on precisely determining intrinsic profiles. Since some spectral features are already below the level of detection in this type of star, their observation in slightly reddened stars is unlikely. Even more reddened stars were also excluded, since such objects are usually faint because of both large distance and high extinction, which leads to difficulties in acquiring high S/N ratios. A variety of rotational velocities also facilitates identification of interstellar features: their profiles should be of the same width irrespective of the stellar rotational speed. Therefore, the rapid rotator BD +40°4220 was included.

4. RESULTS

The prerequisite for a molecule to be identified as a DIB carrier is that a strong origin band in the electronic spectrum must match the DIB wavelength within the experimental uncertainties in the two sets of data. Possible wavelength shifts of the band's maximum due to temperature differences must be taken into account and are discussed in § 5.1. In the following discussion, gas-phase origin bands in the electronic spectra of carbon chains measured in the laboratory (Table 2) are compared to the astronomical observations. DIBs that have been identified with certainty are labeled in the figures as *A* (Herbig 1975), *B* (Krełowski & Sneden 1993; Krełowski et al. 1995, 1997), *C* (Jenniskens & Désert 1994), and *D* (Galazutdinov et al. 2000). Atomic lines (C I, He I, Si IV, C IV) are indicated as well.

4.1. C_6H, C_8H, $C_{10}H$, *and* $C_{12}H$

The linear carbon chain radicals $C_{2n}H$ ($n = 3$–6) show a strong $^2\Pi \leftarrow X^2\Pi$ electronic transition in the optical region, shifting to longer wavelengths with the number of carbon atoms. The laboratory C_6H electronic $^2\Pi \leftarrow X^2\Pi$ transition spectrum is rotationally resolved (Fig. 1), and both spin-orbit components, $\Omega = 3/2$ and 1/2, are visible (Linnartz et al. 1999). The relative intensity of the two spin-orbit components depends on the temperature, which is $\sim$15 K in the spectrum shown. For the larger species, only the lower spin-orbit component transition, $\Omega = 3/2$, is observed, because the spin-orbit splitting is larger in the ground state. The C_8H spectrum (Fig. 2) shows unresolved *P*- and *R*-branches, although the resolution is high enough for individual rotational lines to be discernible (Linnartz et al. 1998). This broadening is caused by intramolecular processes. In the case of $C_{10}H$ and $C_{12}H$ (Figs. 3 and 4), only a broad band could be observed; the sharp lines visible are of pure carbon species, mainly C_2 or C_3, and do not represent the noise level in the laboratory spectra. The band origin

determined from the rotational structure (C_6H) or band maximum (C_8H, $C_{10}H$, or $C_{12}H$) is listed in the second column of Table 2. None of the origin bands in the electronic spectra of these carbon chains, $C_{2n}H$, overlap with absorption features in the astronomical observations. This is also the conclusion when the tabulated DIBs given by Jenniskens & Désert (1994) are used, with the exception of $C_{12}H$. The latter coincides with a DIB listed as "probable" at 7904 Å, but this feature is most likely a stellar line. An inspection of several spectra of heavily reddened stars leads to a negative result: the feature is seen only in star HD 183143, which was the main source of DIBs listed by Jenniskens & Désert (1994); in all other cases it is absent (Fig. 4).

4.2. HC_4H^+, HC_6H^+, *and* HC_8H^+

The origin band of the $^2\Pi \leftarrow X^2\Pi$ electronic transition of the di-, tri- and tetraacetylene cations are compared to the astronomical data in Figures 5, 6, and 7. Each $HC_{2n}H^+$ is isoelectronic with the corresponding $C_{2n}H$ species discussed above, and the electronic transitions lie in a similar wavelength range. These linear cations are centrosymmetric, and thus microwave spectra are not available. Only the $\Omega = 3/2$ component is visible in the 15 K jet spectra ($A'' \sim -30$ cm^{-1}). No distinct DIBs at the laboratory wavelengths (Table 2) are observed. In case of HC_8H^+, a weak DIB observed at 7069.50 Å is close, but does not overlap within a 3 σ uncertainty. The other features are due to He I and Si IV transitions. The origin band of the larger chains will lie beyond 8000 Å.

4.3. NC_4N^+ *and* NC_6N^+

The $^2\Pi \leftarrow X^2\Pi$ electronic origin band of the dicyanodiacetylene and dicyano-triacetylene cation measured in the laboratory is shown in Figures 8 and 9. As for the isoelectronic HC_6H^+ and HC_8H^+ species, these chains have no permanent electric dipole moment and are not accessible to radio astronomy. In the case of NC_6N^+, a comparison is not possible because the region is obscured by a Hα absorption. In the case of NC_4N^+, the resemblance to a DIB at 5959.5 Å is striking (Fig. 8). The structure visible in this DIB resembles an unresolved *P*, *Q*, and *R* branch contour similar to that observed in the laboratory spectrum. However, the wavelengths differ by ~0.9 Å (~2.5 cm^{-1}). Although this is only 0.015% of the absolute frequency of the electronic transition, the bands do not overlap within their 3 σ experimental uncertainties. Because of the similarity in the absorption shapes, the wavelength calibrations of the astronomical (CFHT) and laboratory spectra were carefully checked. The Doppler shift correction for the astronomical spectra was obtained from observations of interstellar Na I, K I and Ca I with accuracy better than 0.1 Å. The laboratory spectrum was calibrated with an accuracy of 0.03 Å using I_2 absorption lines. The possible shift of the band maximum with temperature (see § 5.1) cannot account for a shift of 0.9 Å to a longer wavelength. We conclude that the proximity of these similar band profiles is fortuitous and demonstrates at what level of accuracy agreement between laboratory and astronomical data must be achieved for a definite DIB identification.

4.4. HC_5N^+

Figure 10 shows the rotationally resolved origin band of the $^2\Pi \leftarrow X^2\Pi$ electronic spectrum of the cyanodiacetylene cation, HC_5N^+. The rotational contour of the laboratory spectrum matches a very weak feature at 5818.75 Å obs-

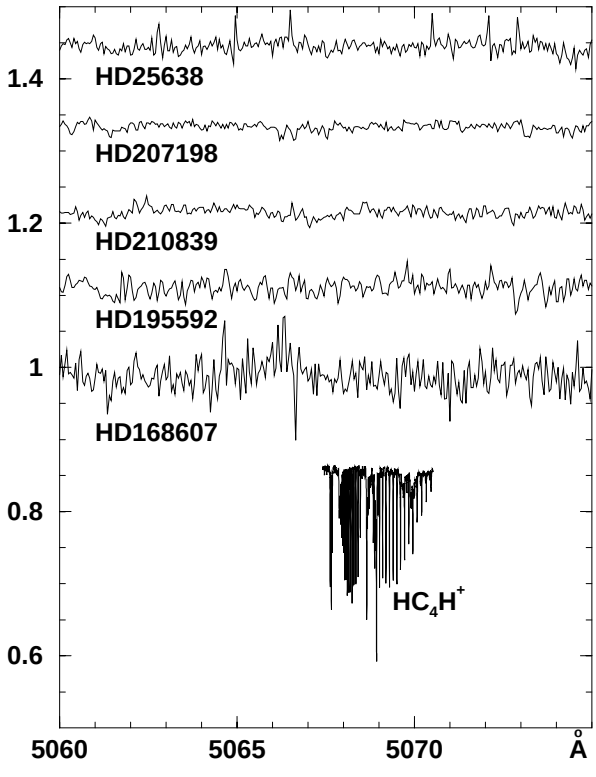

FIG. 5.—Origin band of the $^2\Pi \leftarrow X^2\Pi$ electronic transition of HC_4H^+ in the gas phase (*bottom*) compared to astronomical spectra measured toward five different stars.

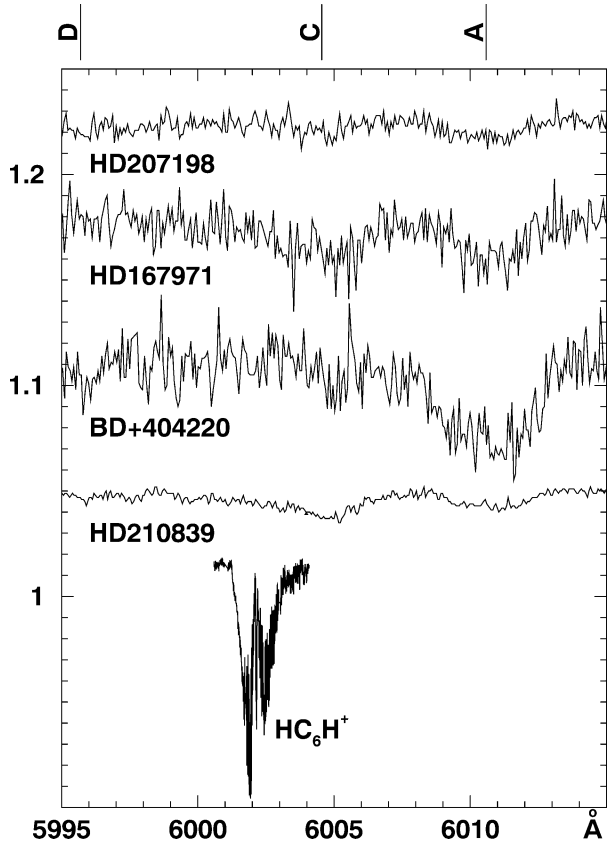

FIG. 6.—Origin band of the $^2\Pi \leftarrow X^2\Pi$ electronic transition of HC_6H^+ in the gas phase (*bottom*) compared to astronomical spectra measured toward four different stars.

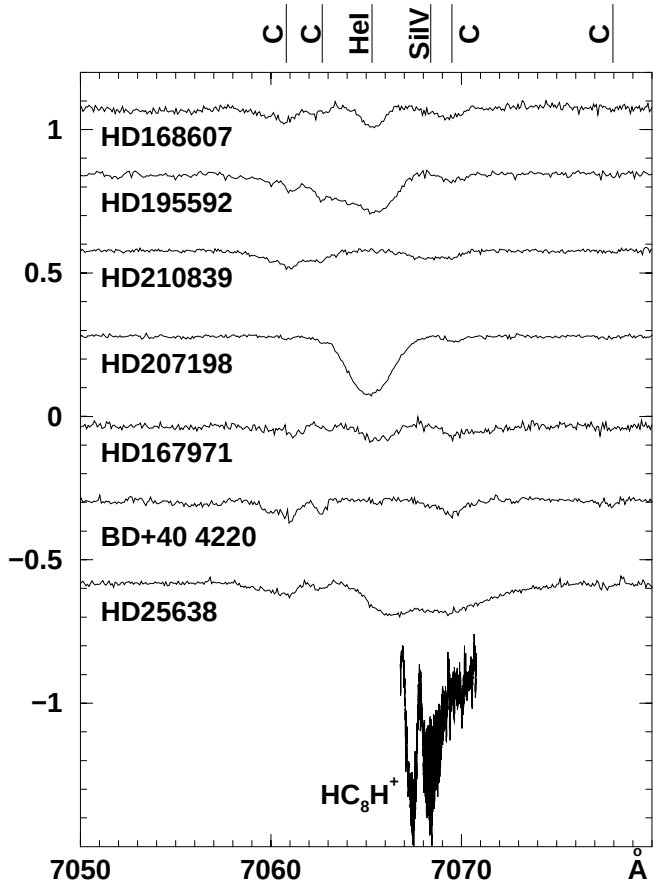

FIG. 7.—Origin band of the $^2\Pi \leftarrow X^2\Pi$ electronic transition of HC_8H^+ in the gas phase (*bottom*) compared to astronomical spectra measured toward seven different stars.

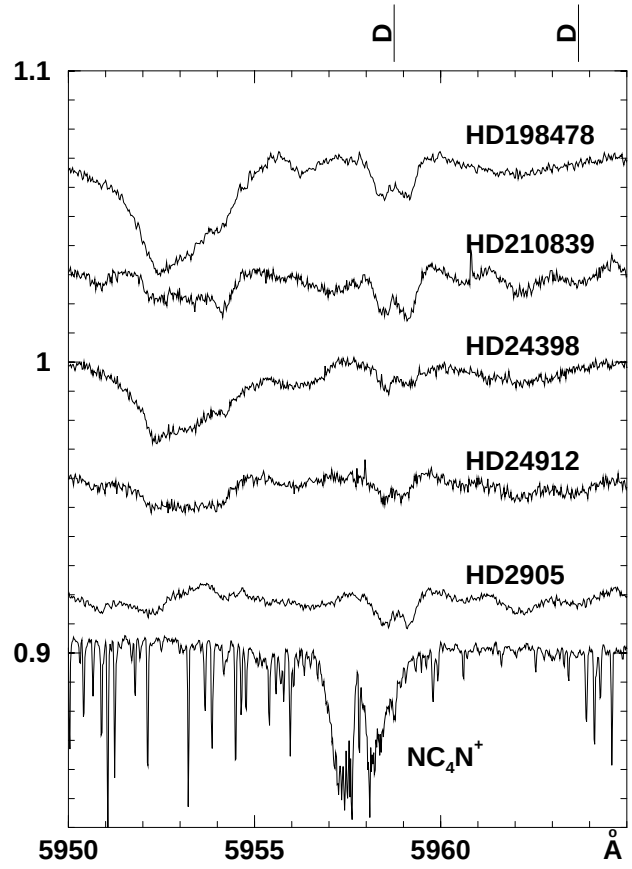

FIG. 8.—Origin band of the $^2\Pi \leftarrow X^2\Pi$ electronic transition of NC_4N^+ in the gas phase (*bottom*) compared to astronomical spectra measured toward five different stars. Absorption features not marked in the latter are stellar lines.

erved both by Jenniskens & Désert (1994) and in the current work, which is shown for three selected stars in Figure 10. The spectra overlap apart from a small shift ($\sim$0.1–0.2 Å). The temperature of the laboratory spectrum is $\sim$15 K. At this stage, the possibility cannot be excluded that the carrier of λ5819 DIB is HC_5N^+, and further astronomical observations are required.

5. DISCUSSION

5.1. *Temperature Dependence*

The profile of molecular absorption bands depends on the population of rotational energy levels in the ground and excited states. Since the intensity of light penetrating the diffuse interstellar medium is far below saturation limit for electronic transitions, the excited state is virtually unpopulated. The rotational structure can be simulated at any temperature, provided that the spectroscopic constants are known for both electronic states. This is the case for many of the chains studied here. Two examples chosen are C_6H and NC_4N^+. The main distinction between these species is that the spin-orbit ground-state splitting for NC_4N^+ ($A'' = -45.0$ cm^{-1}) is nearly 3 times as large as for C_6H ($A'' = -15.04$ cm^{-1}), and that the difference in ground and excited state spin-orbit splittings ($|A'' - A'|$) is considerably larger for C_6H (8.65 cm^{-1}) than for NC_4N^+ (0.53 cm^{-1}). For the simulation of the temperature dependence, the spectroscopic constants given by Linnartz et al. (1999) and Sinclair et al. (1999b) are used. A Gaussian line width of 0.38 cm^{-1} (C_6H) and 0.33 cm^{-1} (NC_4N^+) was taken to smear out the rotational structure. The latter corresponds to $R = 50{,}000$, as used in the astronomical measurements. The result is shown in Figures 11 and 12.

As the temperature increases the spectra broaden, but *P* and *R* branches behave differently. At high temperature, the *R* branch leads to a sharp band head, while the *P* branch becomes shallow and thus difficult to detect. A temperature change induces both a Boltzmann shift in the apparent band maximum and a profile change. However, if the *Q* branch can be distinguished it remains nearly stationary, allowing the most precise wavelength comparison. The second effect is the appearance of the $\Omega = 1/2$ component, which depends on the value of A''. The smaller this value is, the easier it will be to observe the energetically higher component. This is clearly visible in Figures 11 and 12. In addition, the difference $|A'' - A'|$ determines whether the two spin-orbit bands coincide (NC_4N^+) or not (C_6H). In the simulations, a rotational temperature from 3 to 150 K was chosen to cover possible cloud temperatures. For example, the identification of H_3^+ in diffuse clouds led to an estimate of a rotational temperature of 30 K (Geballe et al. 1999). It is expected that polar species such as C_6H cool more effectively than molecules without a permanent electric dipole moment. As can be seen in the case of C_6H and NC_4N^+, the shift of the band's maximum ($\Omega = 3/2$) from 3 to 150 K can be 1 Å to shorter wavelengths.

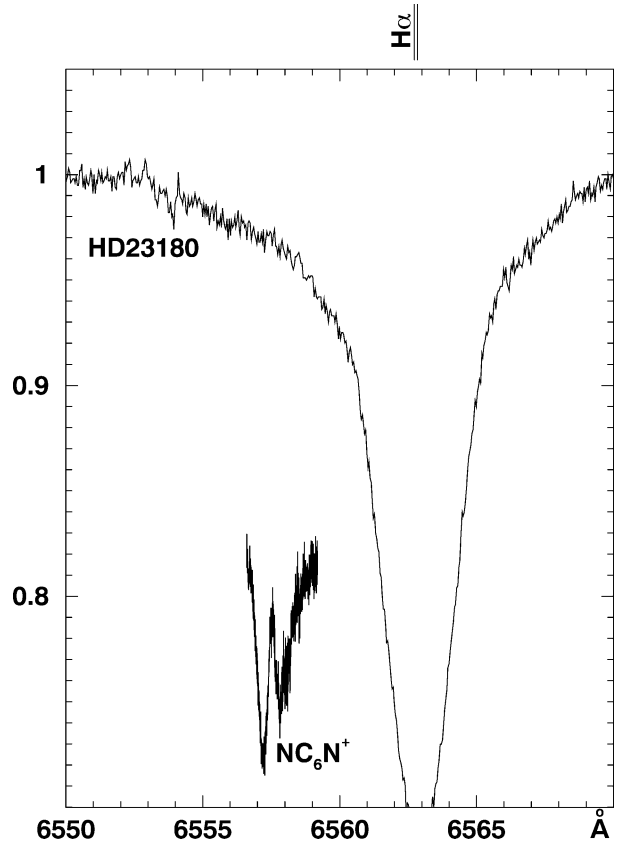

FIG. 9.—Origin band of the $^2\Pi \leftarrow X^2\Pi$ electronic transition of NC_6N^+ in the gas phase. A strong Hα atomic line in the astronomical spectra obscures this region.

5.2. *Column Densities*

The upper limits for the column density of the studied carbon chains in diffuse clouds were inferred as follows. The noise of the astronomical spectra was estimated by fitting a line to the flat section of the baseline and taking the rms of the fit. The detection limit of the equivalent width, W_λ, was calculated via

$$W_{\lambda,\max} = 5 \times \mathrm{FWHM} \times \mathrm{rms}\ ,$$

where FWHM is the full-width at half-maximum for the whole contour and the factor 5 represents an assumed minimum S/N required for detection of a DIB absorption. All these values are given in Table 2. In the case of HC_5N^+, the equivalent width has been estimated for the observed λ5819 DIB. The column density limits were calculated using the standard equation

$$N_{\max} = \frac{4\epsilon_0 m_e c^2}{e^2} \frac{W_{\lambda,\max}}{\lambda^2 f}$$

(in SI units), where the oscillator strength for the origin band of the electronic transition f_{0-0} was estimated from available experimental data. In the case of the $^2\Pi \leftarrow X^2\Pi$ transition of HC_4H^+, $f_{0-0} = 0.04$ is obtained from experimentally measured lifetime and fluorescence yields (Maier & Thommen 1980). In a similar way, $f_{0-0} = 0.06$ is found for HC_6H^+ (Allan, Kloster-Jensen, & Maier 1976). This value is also used for the isoelectronic C_6H, NC_4N^+, and HC_5N^+. For the longer chains, $C_{2n}H$, the f_{0-0} is scaled with the number of carbon and nitrogen atoms, as discussed by Watson (1994). In this way, an upper limit of the column density of the order of 10^{12} cm^{-2} is obtained for the carbon chains discussed here (Table 2).

6. CONCLUSION

The comparison of the laboratory gas-phase spectra of the studied linear carbon chains with astronomical data shows that apart from the origin band of HC_5N^+, there are no matches with DIBs. This does not necessarily mean that these carbon chains are absent in the diffuse interstellar medium, but rather that their column densities are too low to be detected with current observational techniques in the optical region. In fact, pure rotational transitions of several neutral chains, C_2H, C_3H, cyclic C_2H_3, and C_4H, have been detected in absorption in diffuse regions of interstellar space toward a sample of compact extragalactic millimeter-wave continuum sources (Lucas & Liszt 2000), yielding column densities in the 10^{12}–10^{13} cm^{-2} range. These are not much different from those found in dense dark clouds. This may be surprising, because it is often assumed that photodissociation will destroy the smaller species in the diffuse clouds. Since C_6H is likely to be less abundant than C_3H (as it is, for example, in dark clouds by about a factor of 5; Ohishi & Kaifu 1998), N(C_6H) would be $< 10^{12}$ cm^{-2} in diffuse clouds, i.e., below the detection limit given in Table 2.

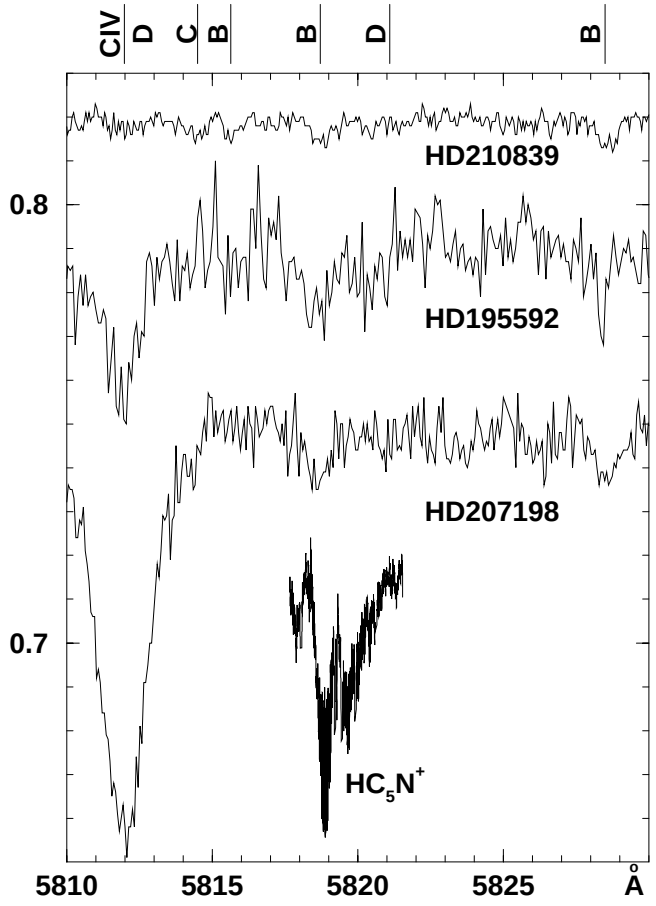

FIG. 10.—Origin band of the $^2\Pi \leftarrow X^2\Pi$ electronic transition of HC_5N^+ in the gas phase (*bottom*) compared to three selected stars. The C IV feature blends a possible DIB. The astronomical spectra show a weak interstellar feature coinciding with the laboratory spectrum.

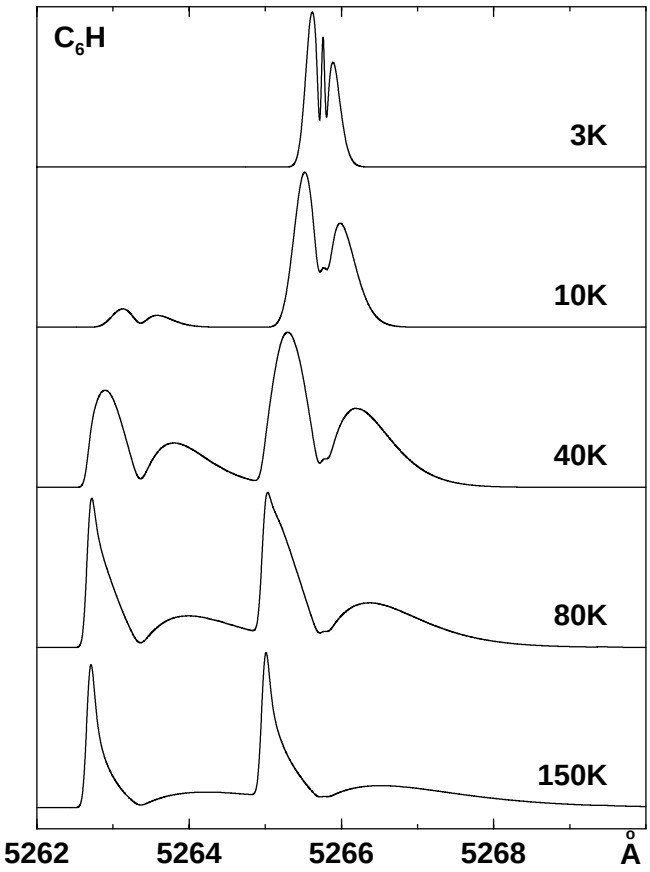

FIG. 11.—Variation of the absorption-band profile of the origin band in the $^2\Pi \leftarrow X^2\Pi$ electronic transition of C_6H with temperature. The simulation uses a resolving power of 50,000.

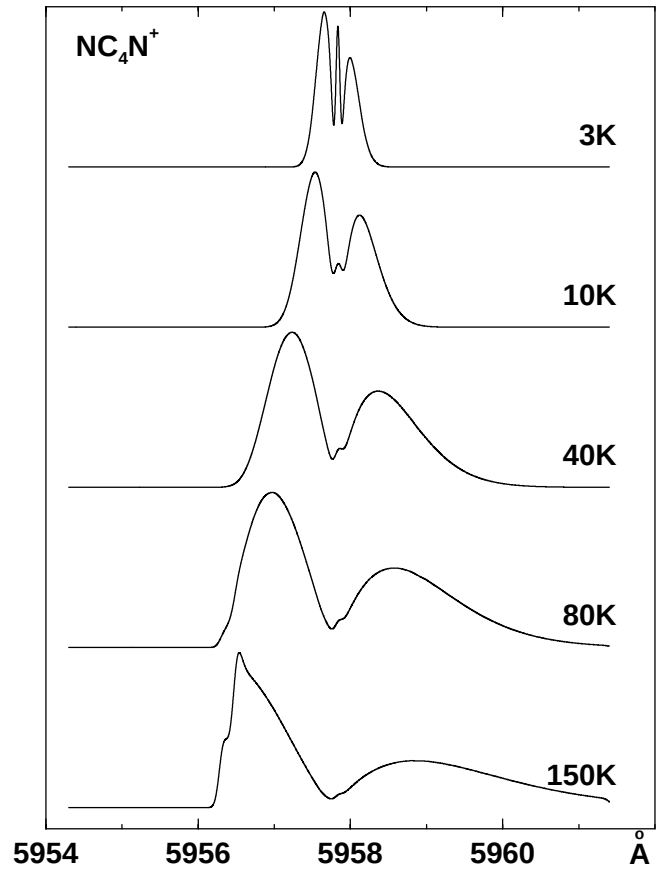

FIG. 12.—Variation of the absorption band profile of a $^2\Pi \leftarrow X^2\Pi$ electronic transition of NC_4N^+ with temperature. A resolution of 50,000 is used in the simulation.

Conversely, the strongest DIBs have an equivalent width W_λ around 10 Å. Assuming an oscillator strength for an electronic transition in the 0.1–1 range would imply a molecule column density of 10^{13}–10^{14} cm^{-2}. Thus, among these carriers, the polar species should be readily observable in absorption by radio astronomy in view of the detections already made.

The authors thank the staff of the Terskol Observatory for help in the acquisition of the astronomical spectra and the Polish National Committee for Scientific Research for financial support from grant 2-P03D-011-15. F. A. M. wants to express his thanks to the Nicolaus Copernicus University in Toruń for supporting his stay at the Center for Astronomy. G. A. G. and F. A. M. acknowledge the partial support of Russian Basic Research Foundation grant 98-02-16544. G. A. H. W.'s research is supported by the Canadian Natural Sciences and Engineering Research Council. D. A. B.'s research is supported by the National Research Council of Canada. The laboratory work in Basel is part of project 20-55285.98 of the Swiss National Science Foundation.

REFERENCES

Allan, M., Kloster-Jensen, E., & Maier, J. P. 1976, Chem. Phys., 7, 11
Beals, C. S., & Blanchet, G. H. 1937, PASP, 49, 224
Crawford, M. K., Tielens, A. G. G. M., & Allamandola, L. J. 1985, ApJ, 293, L45
Douglas, A. E. 1977, Nature, 269, 130
Fulara, J., Lessen, D., Freivogel, P., & Maier, J. P. 1993, Nature, 366, 439
Galazutdinov, G. A. 1992, preprint (Spets. Astrof. Obs. 92)
Galazutdinov, G. A., Krełowski, J., & Musaev, F. A. 1999a, MNRAS, in press
Galazutdinov, G. A., Krełowski, J., Musaev, F. A., Schmidt, M. R., Moutou, C., & d'Hendecourt, L. 1999b, MNRAS, submitted
Galazutdinov, G. A., Musaev, F. A., Krelowski, J., Walker, G. A. M., ApJS, 2000, submitted
Geballe, T. R., McCall, B. J., Hinkle, K. H., & Oka, T. 1999, ApJ, 510, 251
Heger, M. L. 1922, Lick Obs. Bull., 10, 146
Herbig, G. H. 1975, ApJ, 196, 129
Jenniskens, P., & Désert, F.-X. 1994, A&AS, 106, 39
Kerr, T. H., Hibbins, R. E., Fossey, S. J., Miles, J. R., & Sarre, P. J. 1998, ApJ, 495, 941
Krełowski, J., & Schmidt, M. 1997, ApJ, 477, 209
Krełowski, J., Schmidt, M., & Snow, T. P. 1997, PASP, 109, 1135
Krełowski, J., & Sneden, C. 1993, PASP, 105, 1141
Krełowski, J., Sneden, C., & Hiltgen, D. 1995, Planet. Space Sci., 43, 1195
Kroto, H. W., & Jura, M. 1992, A&A, 263, 209
Leger, A., d'Hendecourt, L., & Boccara, N., eds. 1987, Polycyclic Aromatic Hydrocarbons and Astrophysics (Dordrecht: Reidel)
Linnartz, H., Motylewski, T., & Maier, J. P. 1998, J. Chem. Phys., 109, 3819
Linnartz, H., Motylewski, T., Vaizert, O., Maier, J. P., Apponi, A. J., McCarthy, M. C., Gottlieb, C. A., & Thaddeus, P. 1999, J. Mol. Spectrosc., 197, 1
Lucas, R., & Liszt, H. S. 2000, A&A, in press
Maier, J. P. 1982, Accounts Chem. Res., 15, 18
———. 1998, J. Phys. Chem. A, 102, 3462
Maier, J. P., & Thommen, F. 1980, J. Chem. Phys., 73, 5616
McCall, B. J., York, D. G., & Oka, T. 1999, ApJ, 531, this issue
McCarthy, M. C., Travers, M. J., Kovács, A., Gottlieb, C. A., & Thaddeus, P. 1997, ApJS, 113, 105
Merrill, P. W. 1934, PASP, 46, 206
———. 1936, PASP, 48, 179
Merrill, P. W., Sanford, R. F., Wilson, O. C., & Burwell, C. G. 1937, ApJ, 86, 274
Motylewski, T., & Linnartz, H. 1999, Rev. Sci. Instrum., 70, 1305
Musaev, F. A. 1993, Soviet Astron. Lett., 19, 776
———. 1996, Pisma Astron. Zh., 22, 795
Musaev, F. A., Galazutdinov, G. A., Sergeev, A. V., Karpov, N. V., & Podyachev, Y. V. 1999, Kinemat. Fiz. Nebesnyh Tel., in press

Ohara, M., Shiromaru, H., & Achiba, Y. 1997, J. Chem. Phys., 106, 9992
Ohishi, M., & Kaifu, N. 1998, Faraday Discuss., 109, 205
Sinclair, W. E., Pfluger, D., & Maier, J. P. 1999a, J. Chem. Phys., in press
Sinclair, W. E., Pfluger, D., Linnartz, H., & Maier, J. P. 1999b, J. Chem. Phys., 110, 296
Sorokin, P. P., Glownia, J. H., & Ubachs, W. 1998, Faraday Discuss., 109, 137
Tielens, A. G. G. M., & Snow, T. P., eds. 1995, The Diffuse Interstellar Bands (Dordrecht: Kluwer)
Tulej, M., Kirkwood, D. A., Pachkov, M., & Maier, J. P. 1998, ApJ, 506, L69
Watson, J. K. G. 1994, ApJ, 437, 678
York, D. G. 1971, ApJ, 166, 65
Zhao, Y., de Beer, E., Xu, C., Taylor, T., & Neumark, D. M. 1996, J. Chem. Phys., 105, 4905